COBEM 2021 26th International Congress of Mechanical Engineering
November 22-26, 2021, Virtual Congress, Brazil

CCOB-2021-2257

APPLICATIONS OF NEURAL NETWORKS INTO HEAT EXCHANGERS TYPE PCHE

Lucas Rangel Freire
Carolina P. Naveira-Cotta
Nano & Microfluidics and Microsystems, LabMEMS, Mechanical Engineering Dept., POLI & COPPE, UFRJ, Federal University of Rio de Janeiro, Brazil
e-mails: lucas_freire@poli.ufrj.br; carolina@mecanica.coppe.ufrj.br

Abstract. *Printed circuit heat exchangers (PCHEs) are compact and highly effective heat exchangers used from the nuclear industry to offshore gas processing. Despite their advantages, thermal-hydraulic correlations under different geometries and operating conditions are still limited, especially for high Reynolds number flows, therefore hindering optimal designs of these systems. The objective of this work was to apply the neural network's method to predict the impact on the thermohydraulic performance of a heat exchanger, due to changes in the internal geometry of the channels or changes in operating conditions. High computational cost simulations involving the solution of partial differential equations related to the principles of conservation of mass, momentum, and energy were employed in the training of the neural network. The results for the Nusselt number and Fanning friction factor were obtained through the artificial intelligence method and compared with the predictions provided by correlations from the literature and with a complete 3D model solution based on conservations law.*

Keywords: *Printed circuit heat exchanger, Artificial neural network, PCHE, Artificial Intelligence.*

1. INTRODUCTION

The main contribution of this work was the application of Neural Networks technology in predicting the impact on the thermohydraulic performance of a complex heat exchanger. Aiming to demonstrate that, simulated data was used to train the Net, demonstrating the capability of the approach here presented. In a future work real experimental data, not available right now, should be used.

Printed circuit heat exchangers (PCHEs) exemplify the process intensification concept as an alternative to the conventional heat exchangers with advantages, such as higher surface area density, resistance to high pressure and temperature, higher effectiveness, greater compactness, and modularized construction. These advantages made PCHEs broadly used in many industrial applications, such as in supercritical Brayton cycles, offshore oil and gas processing, and the nuclear industry. Among the PCHE geometries, a common design is based on zigzag semi-circular channels. When a fluid flows through a zigzag channel of this type, the thermal boundary layer gets constantly disrupted resulting in heat transfer enhancement compared to the ow in a straight channel. On the other hand, the secondary flows generated near the channel bends also increase the pressure drop. Figure 1 shows a schematic of a PCHE, illustrating the stacking of hot and cold fluid layers, detailing the internal geometries (zigzag angles, and channel pitch), and a 3D view of complete PCHE.

Many researchers have studied thermal-hydraulics aspects of flows in zigzag channels over the past years [1-28]. Some of these works are based on experimental analysis [1-12], while others employed numerical methods [7-28]. A mathematical model based on the physical principles that govern the thermal-hydraulic phenomenon in a PCHE can be built through the laws of conservation (mass, momentum, and energy), written in a differential form that can be very complex and their computational solution's cost can be considered relevant. To overcome this requirement to constantly perform these costly simulations, some correlations have been proposed for the prediction of the heat transfer and pressure drop in PCHE channels some of them listed in Table 1. However, most correlations are valid only for low Reynolds numbers (< 40,000), and the majority of papers in the area focus on supercritical CO2 or helium as working fluids.

Another approach of great interest to surpass this obstacle is the use of Machine Learning-based metamodels. ANN (Artificial Neural Network) has been successfully employed in several applications, not requiring knowledge of the physics of the problem under investigation, having high mapping capabilities and guarantee a good generalization even with a reduced set of identification data, robustness in the presence of poor and/or noisy input data, and characterized by lower computational cost.

In this context, the purpose of this work was to apply the neural network's method to predict the impact on the thermohydraulic performance of a heat exchanger, due to changes in the internal geometry of the channels or changes in operating conditions. This work aims to investigate PCHEs with semicircular zigzag channels for natural gas flow under high Reynolds numbers (40,000 < Re < 100,000), at the hot side of the PCHE, with a water flow at the cold side of the heat exchanger. The effect of the geometric parameter's variation (1 mm < D <5 mm and 15< α <45) on the thermal-hydraulic

performance of the exchanger was evaluated through an artificial intelligence algorithm. The results for the Nusselt number and Fanning friction factor were obtained and compared with correlations and with a complete 3D model solution based on conservations law.

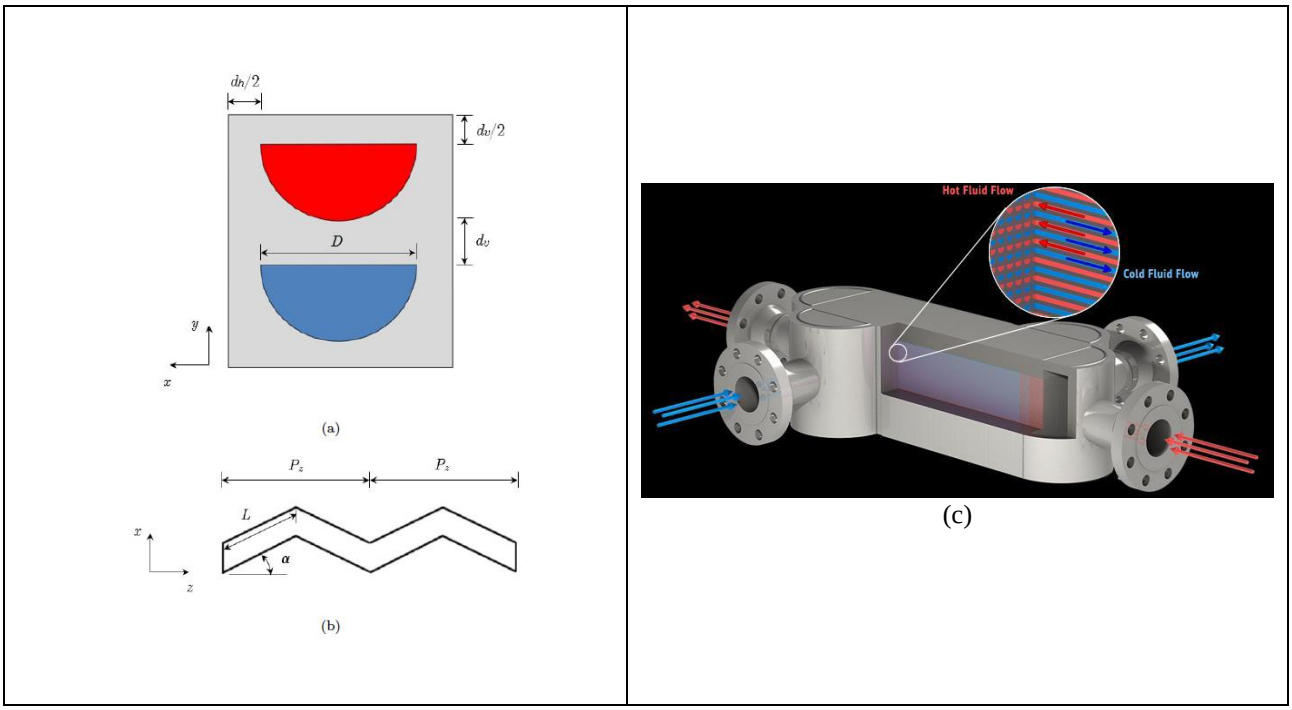

Figure 1. Illustration of PCHE unit (a) cross and (b) longitudinal sections (c) 3D view illustration of a complete PCHE [29]

Table 1 - Numerical correlations for PCHE. [30]

Autor	Correlação Nu e f	Faixas de validade	Fluido	Ângulo	Seção transversal
Berbish *et al.*[30]	$Nu = 0.0228Re^{0.8}$ $f = 0.487Re^{-0.26}$	$8242 \leq Re \leq 57794$	Ar	0° (reto)	Semicirc.
Chen *et al.*[37]	$Nu = (0.01352)Re^{0.080058}$ $Nu = (3.6361 \times 10^{-4})Re^{1.2804}$	$1200 \leq Re \leq 1850$ $1850 < Re \leq 2900$	He-He	15°	Semicirc.
Chen *et al.*[37]	$Nu = (0.047516)Re^{0.633151}$ $Nu = (3.680123 \times 10^{-4})Re^{1.282182}$	$1200 \leq Re \leq 1850$ $1850 < Re \leq 2900$	He-He	15°	Semicirc.
Chen *et al.*[36]	$Nu = (0.05516)Re^{0.69195}$ $f = 17.639Re^{-0.8861}$ $Nu = (0.09221)Re^{0.62507}$ $f = 17.639Re^{-0.8861}$	$1400 < Re \leq 2200$ $2200 < Re \leq 3558$	He-He	15°	Semicirc.
I. Kim *et al.*[29]	$Nu = 3.255 + 0.00729(Re - 350)$ $f \cdot Re = 16.51 + 0.01627Re$	$350 < Re < 800 \quad Pr = 0.66$ $350 < Re < 1200$	He-He	15°	Semicirc.
I. Kim *et al.*[34]	$Nu = 4.089 + 0.00365RePr^{0.58}$ $f \cdot Re = 15.78 + 0.0487Re^{0.84}$ $Nu = 4.089 + 0.00497Re^{0.95}Pr^{0.55}$ $f \cdot Re = 15.78 + 0.0557Re^{0.82}$	$0 < Re < 2500$ $0.66 < Pr < 13.41$ $0 < Re < 3000$ $0.66 < Pr < 13.41$	He-H_2O He-CO_2	15°	Semicirc.

2. CFD

In all simulations, the κ-ω SST turbulence model was used because of its high robustness and because it is the most widely used in the literature for PCHEs. The simulation features the 3D finite volume numerical model, steady-state regime, incompressible fluid assumption, SIMPLE pressure-velocity coupling, 2nd order discretization for pressure, momentum,

and energy. The simulations were performed in the ANSYS Fluent Platform. The assumption of incompressibility was adopted for both fluids, this means that the density is only a function of temperature and not pressure. This hypothesis is reasonable for both fluids since the water is in the liquid phase and the gas presents negligible pressure drop compared to the total pressure at which it is.

The boundary conditions implemented were: (i) fixed total pressure at the inlet of the channels (ii) fixed mass flow rate at the outlet of the channels, (iii) no-slip condition on the channel walls, (iv) fluid-solid conjugate heat transfer on the channel walls, (v) periodic condition on the upper and lower outer walls of the domain, (vi) symmetry condition on the outer sidewalls of the domain, (vii) adiabatic condition on the solid surfaces of the inlet and outlet of the exchanger.

The solid was modeled with constant properties obtained from the ANSYS Fluent library.

In post-processing, a large number of planes parallel to the input (20,000 planes along the complete channel) and perpendicular to the z-direction were used, as shown in Figure 2(b). The choice of these planes over planes perpendicular to the flow direction is based on the greater practicality of generating the planes, coupled with better statistical representativeness of the generated data set. The following local quantities were calculated for each plane in the z-direction:

- Bulk temperature (Tb): average value in the mass flow rate;
- Total pressure (Ptot): average value in the area of each plane;
- Density (ρ): average value in the area of each plane;
- Specific heat (Cp): average value in the area of each plane;
- Viscosity (μ): average value in the area of each plane;
- Thermal conductivity (k): average value in the area of each plane;
- Heat flux in the wall (q''): average value in the line (semicircular wall);
- Wall temperature (Tw): average value in the line (semicircular wall);
- Mass flow rate ($\dot{m}$): average value in the area of each plane.

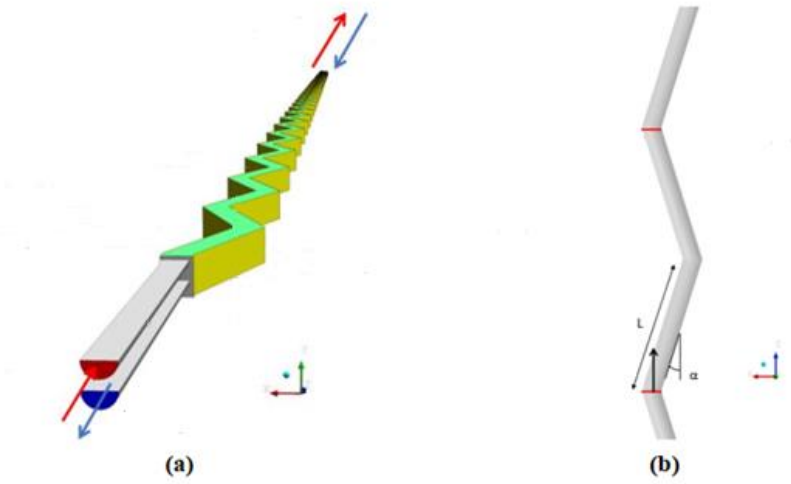

Figure 2. Illustration of the CFD model used. (a) Boundary conditions and (b) post-processing planes. [29]

MESH

An analysis of the convergence of the meshes was performed considering the case where the variation of properties is more pronounced (α = 45º, D = 1 mm, Re = 100,000). The meshes M1, M2, and M3 present, in this order, an increasing number of elements due to the reduction of the characteristic size of each cell in the entire domain (mesh refinement). M2 and M2* meshes differ only in the longitudinal division - while M2 presents equidistant nodes in the longitudinal direction, M2* presents a growth ratio equal to 5 concerning the folds, that is: near the folds, the elements are smaller and as one moves away from them, the elements become larger. This feature proved to be useful in the sense of reducing the total mesh size and better capturing the recirculation effects - which occur in the regions adjacent to the folds.

All the meshes built present refining of the cells belonging to the fluid domain near the walls. This refinement was performed in order to meet the recommendation of the turbulence model used ($y+ \rightarrow 1$). The cross-section and top view of the generated meshes are presented in Figure 3.

The variable analyzed for the convergence analysis was the mean Nusselt number of the hot channel.

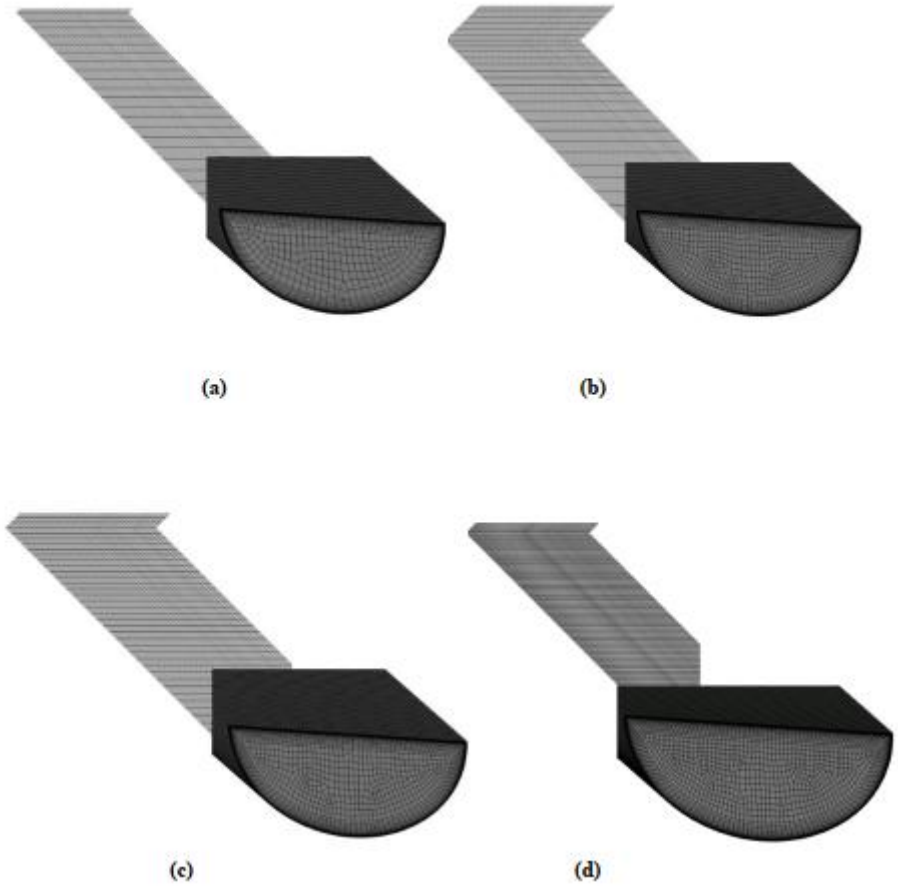

Figure 3. Cross-section and top view of the meshes. **(a)** M1, **(b)** M2, **(c)** M2*, **(d)** M3 [29]

3. METHODOLOGY: ARTIFICIAL INTELLIGENCE

Artificial Neural Networks (ANN) are computational techniques that present a mathematical model inspired by the neural structure of intelligent organisms that acquire knowledge through experience.

An ANN is composed of several processing units, whose operation is quite simple. These units call neurons are connected by communication channels that are associated with a certain weight. The units do operations only on their local data, which are inputs received by their connections. The intelligent behavior of an Artificial Neural Network comes from the interactions between the network's processing units.

Training or learning for neural networks can be classified into two wide groups: supervised and unsupervised learning. In supervised learning, inputs and outputs are known and the ANN model is trained in a way that maps to these inputs and outputs. Supervised learning is employed for regression and classification purposes. However, in unsupervised learning, the outputs are unknown and the hidden relationships in the data set are discovered by the ANN using the data clustering method. Unsupervised learning can be used, for instance, for data filtering, clustering, and data compression

The training step of the Neural Network (i.e., optimization procedure) can be done by different approaches, to list a few: gradient descent-based methods; competitive learning (self-organizing nets); genetic algorithm and concurrent, etc.

An ANN training stage comprises simultaneously, the search for the best network architecture (definition of the number of hidden layers, number of neurons, the type of regularization and activation functions...), and of course, by the respective parameter/weight estimations inherent to these different possibilities of networks, aiming to find the best architecture that gives the best convergence and lower errors.

Before training begins, data should be split into subsets training and validation sets. In this paper the original data were split in training test, made by 90% of data, and the test set, made by the other 10%. Once its architecture has been defined and its respective parameters estimated. The size of these groups can also influence the quality of the network and should also be evaluated in the process of ranking the best ANN. A detailed description of ANN features and capabilities is beyond the scope of the paper: further information can be found in specific literature, such as, among others, [31,32].

In this work to find the best neural network to predict the CFD simulation data set, 1400 different architectures of neural networks were tested combining different numbers of hidden layers, different numbers of neurons per layer, different activation functions, and different approaches of regularization, as informed in Table 2. Ten percent of the total sample was reserved to test the ANNs through the analysis of Mean Square Error (MSE) that was chosen as the error criterion.

Table 2. Parameters for ANN simulations.

PARAMETER	CONDITION	VALUE
Data	Fixed	119
Size of the test set	Fixed	10% of the total amount of data
Regularization	Variable	MinMax or PowerTransformation
Hidden layers	Fixed	2
Neurons	Variable	25 or 50 or 100 or 500 or 1000 or 2000 or 4000
Batch_size	Fixed	32
Epochs	Fixed	200
Transfer function	Variable	Relu, Sigmoid, Tanh, Swish, Elu, Gelu, Selu, Softplus, Softsign e Softmax
Optimization function	Fixed	Adam
Error function	Fixed	MSE

4. RESULTS

In this work, a complete 3D CFD simulation of a PCHE was performed considering a semicircular zigzag channel with natural gas as the hot fluid, water as the cold fluid, varying the channel diameter D between three values: 1, 3, and 5 mm, and zigzag angle α between four values: 15º, 22.5º, 30º, 45º, therefore modifying the zigzag aspect ratio, the number of zigzags and the ratio between the length of half a zigzag and channel hydraulic diameter. Seven Reynolds numbers (40,000; 50,000; 60,000; 70,000; 80,000; 90,000 and 100,000) were simulated for each geometric configuration, and a total of 119 simulations were performed [33].

In the Artificial Neural Networks (ANN) computational procedure 3 parameters as input: Reynolds, angle (α) and the ratio of the length of half a zigzag and channel hydraulic diameter ($\frac{L}{D_h}$). Likewise, as output was considered two parameters, Nusselt and Friction Factor. Figure 4 illustrates the input and output data of the neural network here described.

For the ANN training, a back-propagation algorithm was developed in the Google Colab platform, through a Google GPU, using Python programming language and TensorFlow and Pandas libraries.

As mentioned previously, aiming to find the neural network which best predicts the CFD simulation data set, 1400 different architecture of neural networks were tested, and through the analysis of the MSE error of ten percent of cases, reserved from the complete data set, in particular here, the best-found architecture had considered the MinMax Regularization, two hidden layers with 500 neurons in each, and a Relu activation function was used for both layers. The ADAM optimizer was used, and 200 Epochs were considered. Table 3 shows the 10th best architecture among 1400 tested ANNs and highlight at the first line, which is the best neural networks founded, because of his lowest MSE.

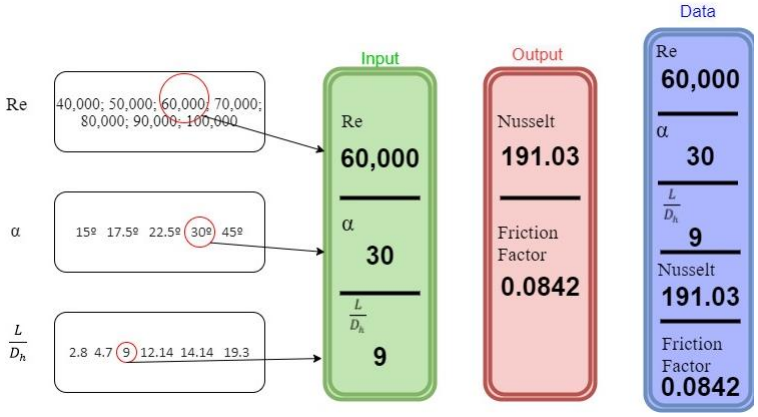

Figure 4. Illustration of the data's parameters.

Table 3. Best tested ANN architectures with two hidden layers, sorted by MSE. Highlighting the chosen one.

Test Set Size (%)	Regularization	Transfer Function	Neurons	Optimizer	Epochs	Train Time	R^2	MSE
10 %	MinMax	Relu/Relu	500	Adam	200	6 s	0.99	0.000176
10 %	MinMax	Relu/Selu	2000	Adam	200	7 s	0.99	0.000202
10 %	MinMax	Selu/Relu	500	Adam	200	6 s	0.99	0.000209
10 %	MinMax	Elu/Relu	2000	Adam	200	7 s	0.99	0.000209
10 %	MinMax	Relu/Elu	500	Adam	200	6 s	0.99	0.000216
10 %	MinMax	Softsign/Relu	2000	Adam	200	7 s	0.99	0.000218
10 %	MinMax	Softsign/Relu	500	Adam	200	6 s	0.99	0.000218
10 %	MinMax	Swish/Relu	1000	Adam	200	7 s	0.99	0.000220
10 %	MinMax	Relu/Tanh	500	Adam	200	6 s	0.99	0.000230
10 %	MinMax	Relu/Elu	4000	Adam	200	8 s	0.99	0.000241

Before training the network, the available data were run through a MinMax transformation function, which is used to handle the order of magnitude of the input variables. Different architectures for the Net was compared, and after all tests the best neural net was the one with two intermediate layers, with the Relu activation function in both layers, 500 neurons in each layer, Adam optimization function to calculate gradients, and 200 epochs.

The same set of data provided by the complete 3D CFD simulation was used to also find the coefficients of a new correlation [33], Eq.1-2, using the Levenberg-Marquart Algorithm, for average Nusselt and average Friction Factor, respectively Eq.1 and 2, both valid in the ranges of $1mm \leq D \leq 5mm;\ 40{,}000 \leq Re \leq 100{,}000;\ 2.8 \leq \frac{L}{D_h} \leq 19.3;\ 15° \leq \alpha \leq 45°$. Where, $Nu_{\alpha=0}$ correspond to the well-known Dittus-Bolters Nusselt correlation for the straight channel (Eq. 3) and $f_{\alpha=0}$ the Blausius friction factor correlation for the straight channel (Eq. 4).

$$\frac{\overline{Nu}}{Nu_{\alpha=0}} = 1 + 0.099\left(\frac{L}{D_h}\right)^{-0.852}\alpha^{1.055}, \tag{1}$$

$$\frac{\bar{f}}{f_{\alpha=0}} = 1 + 0.16\left(\frac{L}{D_h}\right)^{-1.318}\alpha^{2.526}, \tag{2}$$

Dittus-Boelter: $Nu_{\alpha=0} = 0{,}023Re^{0.8}Pr^{0.3}$, (3)
valid for $0.6 \leq Pr \leq 160; Re \geq 10^5; \frac{L}{D_h} > 10$.

Blasius: $f = \frac{0.316}{Re^{0.25}}$, (4)
valid for $4000 < Re < 10^5$.

Tables 4 and 5 compare, respectively, the results of the neural network for the Nusselt number and the Friction Factor, against the proposed correlations (Eq. 1-4) to predict the CFD results.

These 12 cases presented in Tables 4 and 5 are related to the 10% of cases reserved to test the neural network, i.e. they were not used in the training process and were separated for the assessment of its predictive capacity. It is noticed that the

trained network has a better predictive capacity for the Nusselt number, where the minimum, maximum, and average relative deviations found were 0.163%, 4.56%, 2.10% respectively, while for the friction factor there are minimum, maximum, and average errors of 0.947%, 13.238% 5.68% respectively. These Tables also show the best predictive quality of the neural network for both quantities (Nusselt number and friction factor), when compared to the correlation's capability, since q the average deviations of the correlations were 2.77% and 15.43% for respectively Nusselt and friction factor.

Table 4. Comparison of results Nusselt Number

Re	α	$\frac{L}{D_h}$	Nu 3D	Nu ANN	Nu Correl.	Rel. Error ANN (%)	Rel. Error Correl.(%)
40,000	22.5º	4.931	169.723	161.984	165.448	4.560	2.519
40,000	30 º	5.260	186.653	186.349	183.433	0.163	1.725
50,000	22.5 º	4.931	198.657	194.519	197.272	2.083	0.697
60,000	22.5 º	2.958	282.676	301.093	282.873	6.516	0.070
70,000	45 º	9.000	280.237	283.884	285.513	1.302	1.883
70,000	22.5 º	2.958	321.308	334.997	319.816	4.260	0.464
80,000	15 º	14.148	200.314	203.738	211.934	1.709	5.801
90,000	30 º	3.156	489.471	483.116	449.850	1.298	8.095
90,000	17.5 º	12.143	233.799	234.486	241.252	0.294	3.188
100,000	22.5 º	4.931	343.944	340.994	340.987	0.858	0.860
100,000	17.5 º	12.143	254.433	253.769	261.474	0.261	2.767
100,000	15 º	14.148	238.674	243.255	251.081	1.919	5.198

Table 5. Comparison of results Friction Factor

Re	α	$\frac{L}{D_h}$	f 3D	f ANN	f Correl.	Rel. Error ANN (%)	Rel. Error Correl.(%)
40,000	22.5º	4.931	0.026	0.028	0.034	9.388	29.151
40,000	30 º	5.260	0.050	0.043	0.059	13.238	17.455
50,000	22.5 º	4.931	0.024	0.027	0.032	11.667	32.943
60,000	22.5 º	2.958	0.054	0.057	0.055	5.321	0.473
70,000	45 º	9.000	0.076	0.075	0.068	0.947	10.215
70,000	22.5 º	2.958	0.053	0.055	0.052	4.333	0.170
80,000	15 º	14.148	0.007	0.007	0.007	3.338	5.456
90,000	30 º	3.156	0.110	0.109	0.089	1.172	18.563
90,000	17.5 º	12.143	0.010	0.009	0.008	7.377	18.196
100,000	22.5 º	4.931	0.021	0.020	0.027	4.117	25.103
100,000	17.5 º	12.143	0.010	0.009	0.008	5.787	20.060
100,000	15 º	14.148	0.007	0.007	0.006	1.505	7.342

Figure 5 presents the graphical comparisons between the original 3D CFD data points (red dots), the neural network (yellow solid line), and correlation (blue solid line) predictions. The shaded area informs the confidence interval of the predictability of the neural network, considering a confidence level of 95%. For the Nusselt both prediction, ANN and correlation, fits well the original data (black dots), however, for the Friction Factor the neural network shows much better predictability. Figure 6 has a purpose of qualitative Nusselt analysis. It is worth noting that they are all the same figure, only observed from different angles. The black points are the reference values (CFD 3D), the surface was constructed from the neural network for a fixed value of Reynolds number 100,000. In Figure 7 it is possible to observe the behavior of the Nusselt with increasing Reynolds number, as the Reynolds value grows, as expected, the Nusselt number also increases shifting all Nusselt's surfaces up.

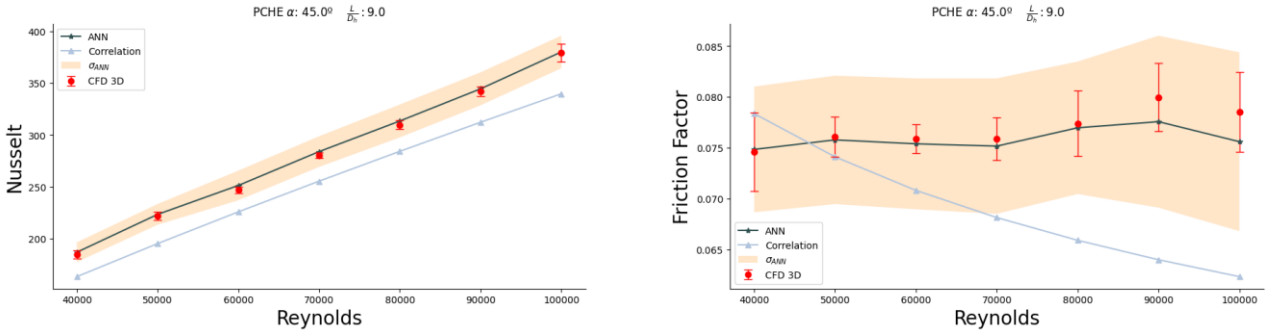

(a) (b)

Figure 5. Comparison of results for Nusselt number (a) and Friction Factor (b).

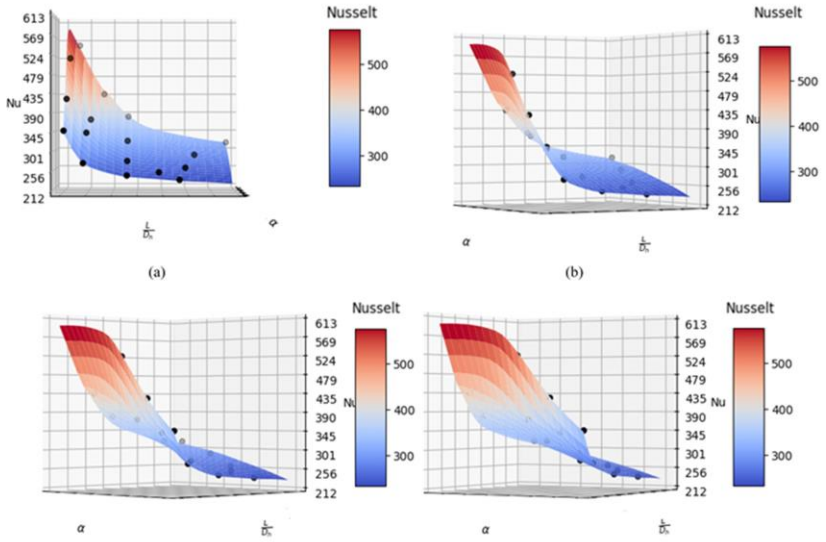

Figure 6. Nusselt plot for Reynolds of 100,000. Figures (a), (b), (c), and (d) represent a rotation around the Z-axis.

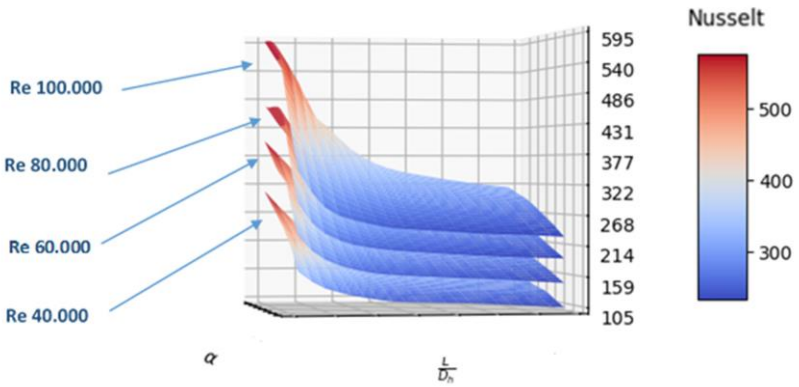

Figure 7. Analysis for four different Reynolds.

5. CONCLUSIONS

The analysis of the operational conditions of the compact heat exchanger with the adoption of neural network models allows predicting the performance of the equipment, even if the internal settings are kept secret by the manufacturer since it is not based on the solution of conservation laws of mass, energy, and momentum.

The neural network approach displays remarkable capabilities to generalize the complex dependence between the variables; this work has presented a fit quite close to the original data set provided by the complete 3D CFD simulation, even not forcing the form of the functional relationship as the correlation function, here proposed, does, being a viable

alternative for predicting Nusselt and friction factor values for heat exchangers type PCHE, thus achieving the initially proposed objective.

The decisive point is that the technique is conditioned on data collection, and the more information added to the data, such as geometric characteristics or other operational measures, the more representative the result will be. It is worth noting that data collection can be done via sensors and as sensors generate a large amount of data, this consequently makes neural networks even more viable.

Also, the neural network could be presented through a Graphical User Interface (GUI), making the neural network available to those who are not familiar with the Python programming language.

Future work could be done using recurrent neural networks (RNN) to describe the transient behavior of a heat exchanger, as these types of neural networks can process a wide variety of dynamic behaviors.

6. REFERENCES

[1] N. S. Berbish, M. Moawed, M. Ammar, R. I. A, Heat transfer and friction factor of turbulent ow through a horizontal semi-circular duct, Heat and Mass Transfer 47 (4) (2011) 377{384. doi:10.1007/s00231-010-0727-y.

[2] A. Katz, S. R. Aakre, M. H. Anderson, D. Ranjan, Experimental investigation of pressure drop and heat transfer in high-temperature supercritical CO2 and helium in a printed-circuit heat exchanger, International Journal of Heat and Mass Transfer 171 (2021) 121089. doi: 10.1016/j.ijheatmasstransfer.2021.121089.34

[3] M. Chen, X. Sun, R. N. Christensen, I. Skavdahl, V. Utgikar, P. Sabhar, Pressure drop and heat transfer characteristics of a high-temperature printed circuit heat exchanger, Applied Thermal Engineering 108 (2016) 1409{1417. doi:10.1016/j.applthermaleng.2016.07.149.

[4] K. Nikitin, Y. Kato, L. Ngo, Printed circuit heat exchanger thermal-hydraulic performance in supercritical CO2 experimental loop, International Journal of Refrigeration 29 (5) (2006) 807-814. doi:10.1016/j.ijrefrig.2005.11.005.

[5] W. Chu, X. Li, Y. Chen, Q. Wang, T. Ma, Experimental Study on Small Scale Printed Circuit Heat Exchanger with Zigzag Channels, Heat Transfer Engineeringdoi:10.1080/01457632.2020.1735779.

[6] K. Cheng, J. Zhou, H. Zhang, X. Huai, J. Guo, Experimental investigation of thermal-hydraulic characteristics of a printed circuit heat exchanger used as a pre-cooler for the supercritical CO2 Brayton cycle, Applied Thermal Engineering 171 (2020) 115116. doi:10.1016/j.applthermaleng.2020.115116.

[7] M. Chen, X. Sun, R. N. Christensen, Thermal-hydraulic performance of printed circuit heat exchangers with zigzag ow channels, International Journal of Heat and Mass Transfer 130 (2019) 356{367. doi:10.1016/j. ijheatmasstransfer.2018.10.031.

[8] I. H. Kim, H. C. No, J. I. Lee, B. G. Jeon, Thermal hydraulic performance analysis of the printed circuit heat exchanger using a helium test facility and CFD simulations, Nuclear Engineering and Design 239 (11) (2009) 2399-2408. doi:10.1016/j.nucengdes.2009.07.005.

[9] I. H. Kim, H. C. No, Thermal hydraulic performance analysis of a printed circuit heat exchanger using a helium-water test loop and numerical simulations, in Applied Thermal Engineering, Vol. 31, Pergamon, 2011, pp. 4064-4073. doi:10.1016/j.applthermaleng.2011.08.012.35

[10] I. H. Kim, H. C. NO, Thermal-hydraulic physical models for a Printed Circuit Heat Exchanger covering He, He-CO2 mixture, and water fluids using experimental data and CFD, Experimental Thermal and Fluid Science 48 (2013) 213{221. doi:10.1016/j.expthermflusci.2013.03.003.

[11] M. Chen, X. Sun, R. N. Christensen, I. Skavdahl, V. Utgikar, P. Sabharwall, Dynamic behavior of a high-temperature printed circuit heat exchanger: Numerical modeling and experimental investigation, Applied Thermal Engineering 135 (2018) 246{256. doi:10.1016/j.applthermaleng.2018.02.051.

[12] S. Baik, S. G. Kim, J. Lee, J. I. Lee, Study on CO2 water printed circuit heat exchanger performance operating under various CO phases for S-CO power cycle application, Applied Thermal Engineering 113 (2017) 1536-1546. doi:10.1016/j.applthermaleng.2016.11.132.

[13] S. G. Kim, Y. Lee, Y. Ahn, J. I. Lee, CFD aided approach to design printed circuit heat exchangers for supercritical CO2 Brayton cycle application, Annals of Nuclear Energy 92 (2016) 175{185. doi:10.1016/j.anucene.2016.01.019.

[14] Optimization and heat transfer correlations development of zigzag channel printed circuit heat exchangers with helium fluids at high temperature, International Journal of Thermal Sciences 160 (2021) 106645. doi:10. 1016/j.ijthermalsci.2020.106645.

[15] Thermal Performance Analysis in a Zigzag Channel Printed Circuit Heat Exchanger under Different Conditions, Heat Transfer Engineeringdoi:10.1080/01457632.2021.1896832.

[16] I. H. Kim, X. Sun, CFD study and PCHE design for secondary heat exchangers with FLiNaK-Helium for SmAHTR, Nuclear Engineering and Design 270 (2014) 325{333. doi:10.1016/j.nucengdes.2014.02.003.36

[17] S. M. Lee, K. Y. Kim, Comparative study on performance of a zigzag printed circuit heat exchanger with various channel shapes and configurations, Heat and Mass Transfer 49 (7) (2013) 1021{1028. doi:10.1007/s00231-013-1149-4.

[18] T. Ma, L. Li, X. Y. Xu, Y. T. Chen, Q. W. Wang, Study on local thermal-hydraulic performance and optimization of a zigzag-type printed circuit heat exchanger at high temperature, Energy Conversion and Management 104 (2015) 55{66. doi:10.1016/j.enconman.2015.03.016.

[19] T. Ma, M. J. Li, J. L. Xu, F. Cao, Thermodynamic analysis and performance prediction on dynamic response characteristic of PCHE in 1000 MW S-CO2 coal _red power plant, Energy 175 (2019) 123{138. doi:10.1016/j.energy.2019.03.082.
[20] A. Meshram, A. K. Jaiswal, S. D. Khivsara, J. D. Ortega, C. Ho, R. Bapat,P. Dutta, Modeling and analysis of a printed circuit heat exchanger for supercritical CO2 power cycle applications, Applied Thermal Engineering 109 (2016) 861-870. doi:10.1016/j.applthermaleng.2016.05.033.
[21] J. Pan, J. Wang, L. Tang, J. Bai, R. Li, Y. Lu, G. Wu, Numerical investigation on thermal-hydraulic performance of a printed circuit LNG vaporizer, Applied Thermal Engineering 165 (2020) 114447. doi:10.1016/j.applthermaleng.2019.114447.
[22] S. H. Yoon, H. C. NO, G. B. Kang, Assessment of straight, zigzag, S-shape, and airfoil PCHEs for intermediate heat exchangers of HTGRs and SFRs, Nuclear Engineering and Design 270 (2014) 334-343. doi:10.1016/j.nucengdes.2014.01.006.
[23] S. J. Yoon, J. O'Brien, M. Chen, P. Sabharwall, X. Sun, Development and validation of Nusselt number and friction factor correlations for laminar in a semi-circular zigzag channel of printed circuit heat exchanger,
Applied Thermal Engineering 123 (2017) 1327{1344. doi:10.1016/j.applthermaleng.2017.05.135.37
[24] S. M. Lee, K. Y. Kim, A parametric study of the thermal-hydraulic performance of a zigzag printed circuit heat exchanger, Heat Transfer Engineering 35 (13) (2014) 1192{1200. doi:10.1080/01457632.2013.870004. URL https://www.tandfonline.com/doi/abs/10.1080/01457632. 2013.870004
[25] J. H. Kim, S. Baek, S. Jeong, J. Jung, Hydraulic performance of a microchannel PCHE, Applied Thermal Engineering 30 (14-15) (2010) 2157-2162. doi:10.1016/j.applthermaleng.2010.05.028.
[26] K. Bennett, Y. tung Chen, Printed circuit heat exchanger performance analysis using non-uniform segmental design method, Applied Thermal Engineering 153 (2019) 69{84. doi:10.1016/j.applthermaleng.2019. 02.102.
[27] D. E. Kim, M. H. Kim, J. E. Cha, S. O. Kim, Numerical investigation on thermal{hydraulic performance of new printed circuit heat exchanger model, Nuclear Engineering and Design 238 (12) (2008) 3269-3276. doi:10.1016/j.nucengdes.2008.08.002.
[28] T. Ma, U. Pasquier, Y. Chen, Q. Wang, Numerical study on thermal-hydraulic performance of a two-sided etched zigzag-type high-temperature printed circuit heat exchanger, in Energy Procedia, Vol. 142, Elsevier Ltd, 2017, pp. 3950-3955. doi:10.1016/j.egypro.2017.12.302.
[29] S. Aakre, I. Jentz, M. Anderson, Nuclear code case development of printed-circuit heat exchangers with thermal and mechanical performance testing (2018).
[30] A. C. P. Oliveira, "ANÁLISE NUMÉRICA DE TROCADOR DE CALOR DO TIPO CIRCUITO IMPRESSO (PCHE) APLICADO A REATOR DE FUSÃO NUCLEAR," MSc Dissertation on Nuclear Engineering, COPPE/UFRJ, Rio de Janeiro, 2020.
[31] A. Gulli, A. Kapoor, S. Pal, Deep Learning with TensorFlow 2 and Keras: Regression, ConvNets, GANs, RNNs, NLP, and More with TensorFlow 2 and the Keras API, 2nd Edition, ISBN 1838823417, 9781838823412, Packt Publishing, (2019).
[32] A. Géron, Hands-On Machine Learning with Scikit-Learn and TensorFlow, Publisher(s): O'Reilly Media, Inc.
ISBN: 9781491962299, (2017).
[33] C. P. Naveira-Cotta, S. Jian, et. al, Relatório Tecnico Projeto PEM 20058 - CENPES/COPPE, “Analise teorico-experimental de permutadores de calor do tipo circuito impresso”, Rio de Janeiro, 2017-2020.

7. RESPONSIBILITY NOTICE

The authors Lucas R. Freire and Carolina P. Naveira-Cotta are the only ones responsible for the printed material included in this paper.

8. ACKNOWLEDGMENT

This work was accomplished with partial financial support from Petrobras and the research sponsoring agencies CNPq and FAPERJ.